Macromolecules

Article

pubs.acs.org/Macromolecules

Thermodynamic Interactions and Phase Behavior of Multicomponent Blends Containing Supercritical Carbon Dioxide, Styrene–Acrylonitrile Random Copolymer, and Deuterated Poly(methyl methacrylate)

Nicholas P. Young,[†] Sebnem Inceoglu,[‡] Gregory M. Stone,[§] Andrew J. Jackson,[∥] Steven R. Kline,[⊥] Stéphane Costeux,[#] and Nitash P. Balsara*[,†,‡,&]

[†]Department of Chemical and Biomolecular Engineering, University of California, Berkeley, Berkeley, California 94720, United States

[‡]Materials Sciences Division and [&]Environmental Energy Technologies Division, Lawrence Berkeley National Laboratory, Berkeley, California 94720, United States

[§]Malvern Instruments Inc., 117 Flanders Road, Westborough, Massachusetts 01581, United States

[∥]European Spallation Source ESS AB, Lund SE-221 00, Sweden

[⊥]NIST Center for Neutron Research, Gaithersburg, Maryland 20899-6102, United States

[#]The Dow Chemical Company, Dow Building & Construction, Midland, Michigan 48674, United States

Supporting Information

ABSTRACT: Small-angle neutron scattering (SANS) was used to probe the phase behavior of multicomponent mixtures of supercritical carbon dioxide ($scCO_2$), styrene–acrylonitrile random copolymer, and deuterated poly(methyl methacrylate). Ternary mixtures were homogeneous at low carbon dioxide pressures (P_{CO_2}) but phase separated as P_{CO_2} was increased at constant temperature (T). Phase separation pressure was found to be a nonmonotonic function of T with a minimum at T = 60 °C. An expression based on the multicomponent random phase approximation was used to determine the interaction parameters between polymer and $scCO_2$ from a combination of SANS experiments on homogeneous ternary mixtures and measurements of $scCO_2$ uptake by the neat polymers. Interaction parameters that underlie the nonmonotonic phase behavior described above collapse onto a straight line when plotted as a function of $scCO_2$ density.

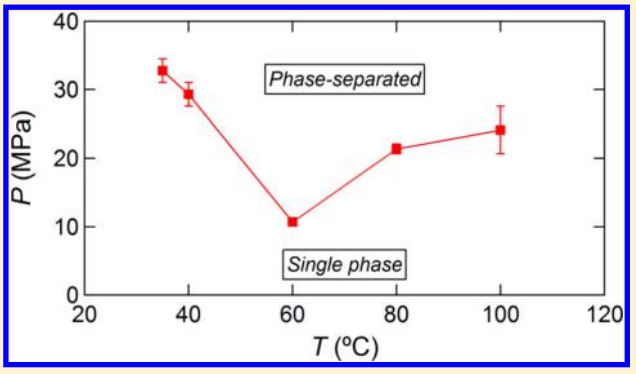

1. INTRODUCTION

In a previous publication, we described a framework for analyzing the small-angle neutron scattering (SANS) profiles obtained from single-phase mixtures of two polymers and supercritical carbon dioxide ($scCO_2$) based on the multicomponent random phase approximation (RPA).[1] This, in combination with solubility of the individual polymers in $scCO_2$, enabled quantifying the Flory–Huggins interaction parameters between $scCO_2$ and the two polymers in a particular multicomponent blend. The experimental work in ref 1 was performed on styrene–acrylonitrile random copolymer (SAN) and deuterated poly(methyl methacrylate) (dPMMA), and that study was restricted to a particular temperature (40 °C). In this paper, we study the same SAN/dPMMA/$scCO_2$ blend over a range of temperatures (T) and $scCO_2$ pressures (P_{CO_2}). At all values of T studied, increasing P_{CO_2} results in macrophase separation. The phase separation pressure ($P_{CO_2,s}$) decreases with increasing T when T < 60 °C but increases with increasing T at higher temperatures. In this paper, we explore the relationship between phase behavior and the Flory–Huggins parameters determined from the homogeneous ternary blend. As one might expect, the Flory–Huggins interaction parameters between $scCO_2$ and the polymers exhibit complex behaviors when plotted against T or P_{CO_2}. Surprisingly, the interaction parameters collapse onto a straight line when plotted against the density of the $scCO_2$.

2. EXPERIMENTAL SECTION

Materials. The SAN copolymer utilized in this study was prepared using methods described in ref 1. The obtained copolymer was named following the nomenclature SAN*XX*(*yy*), where *XX* and *yy* are the total

Received: September 1, 2014
Revised: October 24, 2014
Published: November 7, 2014

   dx.doi.org/10.1021/ma5018154 | Macromolecules 2014, 47, 8089–8097

weight-averaged molecular weight M_w in kg/mol of the copolymer and weight percentage of acrylonitrile ($100w_{AN}$) in the copolymer, respectively, where w_{AN} is the weight fraction of acrylonitrile in the copolymer. A dPMMA sample was purchased from Polymer Source and freeze-dried from a benzene−tetrahydrofuran (THF) mixture prior to use.[2] This polymer is referred to as dPMMA*ZZ*, where *ZZ* is M_w in kg/mol. In order to more precisely determine the molecular characteristics of the polymers in this study, we performed gel permeation chromatography (GPC) characterization using triple detection via refractive index, viscosity, and light scattering. This allowed the measurement of absolute molecular weight in terms of the numbered-averaged molecular M_w as well as the polydispersity index (PDI = M_w/M_n). Polymers were analyzed by a Malvern Instruments Viscotek TDA 305 GPC system with a single T-6000 M mixed bed column. The system used THF as eluent at 30 °C with a flow rate of 1 mL/min. In ref 1, we reported and used the molecular weight of dPMMA as specified by Polymer Source (125 kg/mol). In this paper, we use the value obtained by our analysis, which found M_w = 190 kg/mol and PDI = 1.03. While this difference affects the quantitative analysis, none of the major conclusions reported in ref 1 are affected by this change.

Throughout this paper, the components will be referred to according to the following numerical nomenclature: 1 = $scCO_2$, 2 = SAN, and 3 = dPMMA (or, in some cases, hydrogenous PMMA). The effective degree of polymerization with respect to a reference volume v_0 of 0.1 nm^3 is $N_i = M_{w,i}v_i/(M_{0,i}v_0)$. The monomer molecular weight $M_{0,i}$ are $M_{0,S}$ = 104.15 g/mol, $M_{0,AN}$ = 53.06 g/mol, and $M_{0,3}$ = 108.17 g/mol. The monomer volumes v_i at a reference temperature T_{ref} = 413.15 K and a reference pressure P_{ref} = 0.1 MPa are v_S = 0.179 nm^3,[3] v_{AN} = 0.0819 nm^3,[4] and v_3 = 0.149 nm^3.[3] The dependence of v_i on T is obtained from the thermal expansion coefficient, d ln v_i/dT, for which we use an approximate value of 7×10^{-4} K^{-1}.[3] We ignore the heterogeneous nature of SAN copolymer chains and obtain average $M_{0,SAN}$ and v_{SAN} from the mass and volume averages of the constituent values, respectively. We thus obtain values of $M_{0,2}$ = 90.87 g/mol and v_2 = 0.156 nm^3. The statistical segment lengths of dPMMA ($l_{3,ref}$) and SAN ($l_{2,ref}$) at the reference conditions are 0.54 and 0.83 nm, respectively.[3,1] Table 1 lists the characteristics of the two polymers, including M_w, PDI, w_{AN}, and N.

Table 1. Polymer Characteristics

polymer	M_w (kg/mol)	PDI	w_{AN}	N
SAN87(26)	87	1.17	26	1045
dPMMA190	190	1.03		1757

Blend Film Preparation. SAN/dPMMA blends were prepared by drop-casting. Predetermined quantities of dPMMA190 and SAN87(26) polymers needed to achieve the desired blend composition of $\phi_{3,0}$ = 0.461 were dissolved in THF (~0.2 g/mL) and stirred for 2 days to obtain a homogeneous solution. The volume fraction of component i in the $scCO_2$-free polymer mixture is $\phi_{i,0}$ ($\phi_{1,0}$ = 0, $\phi_{2,0}$ = 0.539, and $\phi_{3,0}$ = 0.461). The volume fraction was determined using the polymer density in the amorphous state, $\rho_i = M_{0,i}/v_i$, and the weight fraction, w_i, of the polymers in the $scCO_2$ mixture. Films were prepared by slowly drop-casting the solution inside O-rings (McMaster Compressible FEP-Encapsulated Silicone O-Rings: nominal thickness = 1/16 in.) to avoid the formation of air bubbles and subsequently dried at ambient T and pressure (P) for 4 days and under vacuum at room temperature for 2 days. The thickness t of the films was controlled between 80 and 200 μm by varying the quantity of solution dropped into the O-ring spacer. The resulting films were measured with a micrometer at least five times to get an average value of t.

Solubility Measurements. A typical experimental magnetic suspension balance (MSB) setup is described by Areerat et al.[5] The sample (mass m_p ~ 1.3 g, diameter d = 19 mm diameter,and t = 2.5 mm) was introduced into the chamber in a nonmagnetic stainless steel basket, itself attached to the magnetic suspension. The sample chamber was heated to the desired temperature under vacuum with an oil bath (Julabo F26-ME). Upon equilibration, $scCO_2$ was introduced using a syringe pump (Teledyne Isco, Model 500D). Pressure was increased by steps, and the sample was allowed to equilibrate until the apparent mass uptake m_a reaches a stable value. The experimental definition of m_a is given by

$$m_a = m_g - \rho_f(V_b + V_{mix}) \quad (1)$$

where m_g is the actual mass of gas absorbed by the polymer sample, ρ_f is the density of the fluid, V_b is the volume of the bucket, and V_{mix} is the volume of the $scCO_2$-swollen polymer sample.

Determination of the true absorbed mass requires knowledge of V_{mix} that has the density of the $scCO_2$-swollen polymer. The perturbed chain statistical associating field theory (PC-SAFT) equation of state (EoS) can be used to determine the gas composition and density of the swollen polymer simultaneously at all pressures and temperatures by regressing PC-SAFT binary interaction parameters k_{ij} between $scCO_2$ and polymers to the apparent mass:

$$m_a = m_p\frac{w_{1-i}}{1-\rho_{mix}} - \rho_f\left[V_b + \frac{m_p}{(1-w_{1-i})\rho_{mix}}\right] \quad (2)$$

where w_{1-i} is the PC-SAFT predictions for $scCO_2$ fraction in the swollen polymer i and ρ_{mix} is the swollen polymer density.

PC-SAFT is a statistical-mechanics-based EoS in which molecules are modeled as chains of tangentially connected spherical segments.[6] The Helmholtz free energy (A) of a chain molecule is written as a perturbation expansion starting from spherical segments and then adding the contribution due to chain connectivity as a perturbation term. The only parameters needed are for segments and can be classified either as pure component or as binary interaction parameters. The pure component parameters are segment diameter (σ), number of segments in the chain (m), and dispersion energy (ε/k) are listed in Table 2. In addition to these, there is an adjustable

Table 2. PC-SAFT EoS Pure Component Parameters

component	m/M	σ (nm)	ε/k (K)
$scCO_2$	0.0471	0.288	169.2
MMA	0.0262	0.360	245.0
S	0.0334	0.349	292.6
AN	0.0333	0.327	270.3

binary parameter k_{ij} that is fitted to match the binary phase equilibrium data (vapor−liquid or liquid−liquid equilibrium) of a pair of compounds. Linear dependence of k_{ij} on T given by $k_{ij} = k_{a,ij} + Tk_{b,ij}$ was found to be adequate to account for the association interaction between $scCO_2$ and PMMA. Parameter regressions and solubility predictions were performed using VLXE, a commercial implementation of the PC-SAFT EoS (VLXE ApS, Copenhagen, Denmark). In VLXE, copolymers are handled as chain of effective segments with monomer composition equal to the chain average composition. Thus, predictions for SAN are obtained by regressing parameters for PS and PAN. Binary interaction between styrene and acrylonitrile are ignored. Parameters for the interactions between $scCO_2$ and each monomer are listed in Table 3.

Small-Angle Neutron Scattering. SANS measurements were carried out on the NG3 and NG7 beamlines at the National Institute of Standards and Technology Center for Neutron Research (NCNR) in Gaithersburg, MD. We added $scCO_2$ to the blend using a modified

Table 3. PC-SAFT Binary Interaction Parameter Coefficients

binary	$k_{a,ij}$	$k_{b,ij}$ (K^{-1})
$scCO_2$/PMMA	−0.0776	0.000489
$scCO_2$/PS	−0.0441	0.000282
$scCO_2$/PAN	0.008 71	0.000

dx.doi.org/10.1021/ma5018154 | Macromolecules 2014, 47, 8089−8097

high-P_{CO_2} sample environment provided by NCNR, the details of which have been described previously.[1] Each blend was thermally equilibrated at the desired T for 30 min prior to addition of $scCO_2$, and the sample cell was flushed with CO_2 before pressurization by opening a valve in series with the cell. The valve was then closed, and the piston was adjusted to obtain the desired P_{CO_2}. SANS data were obtained using the following protocol: upon equilibration of the sample with the $scCO_2$ reservoir at the desired P_{CO_2}, a series of three 2 min runs were commenced, followed by a 3 min transmission run. This series of runs was repeated one time, for a total of 12 min of scattering data collection. If time-independent scattering profiles were obtained, the P_{CO_2} was increased to the next value and the process was repeated. In some cases, especially near the point of phase separation, the sequence of scattering and transmission runs would be repeated more than twice until equilibrium scattering profiles were obtained or clear evidence of phase separation was observed. Raw data were corrected for detector sensitivity,[7] background and empty cell scattering contributions, incoherent scattering, and coherent scattering from the pure dPMMA as well as to correct for the change in t when swollen with $scCO_2$.[8] Data were azimuthally integrated to obtain absolute scattering intensity, I, as a function of the scattering vector, q, where $q = (4\pi/\lambda)\sin(\theta/2)$, λ is the incident neutron beam wavelength (0.6 nm), and θ is the scattering angle. All $scCO_2$ experiments were conducted using a sample-to-detector distance of 5 m, to obtain a q range of $0.133\ \text{nm}^{-1} \le q \le 0.886\ \text{nm}^{-1}$.

3. THEORY OF SCATTERING FROM HOMOGENEOUS MULTICOMPONENT MIXTURES

The expression for $I(q)$ for the multicomponent mixtures of interest derived in ref 1 is

$$I(q) = B_1^2 S_{11}(q) + 2B_1B_2S_{12}(q) + B_2^2 S_{22}(q) \tag{3}$$

$$S_{11}(q) = \frac{\frac{1}{S_{22}^\circ} + V_{22}}{\left(\frac{1}{S_{11}^\circ} + V_{11}\right)\left(\frac{1}{S_{22}^\circ} + V_{22}\right) - V_{12}^2} \tag{4}$$

$$S_{22}(q) = \frac{\frac{1}{S_{11}^\circ} + V_{11}}{\left(\frac{1}{S_{11}^\circ} + V_{11}\right)\left(\frac{1}{S_{22}^\circ} + V_{22}\right) - V_{12}^2} \tag{5}$$

$$S_{12}(q) = \frac{-V_{12}}{\left(\frac{1}{S_{11}^\circ} + V_{11}\right)\left(\frac{1}{S_{22}^\circ} + V_{22}\right) - V_{12}^2} \tag{6}$$

where B_{i3} is the scattering contrast between components i and 3:

$$B_{i3} = \frac{b_i}{v_i} - \frac{b_3}{v_3} \quad (i = 1,\ 2) \tag{7}$$

with b_i and v_i representing the scattering length and the monomer volume of component i, respectively, and their ratio is the scattering length density.

$$S_{ii}^\circ(q) = N_i\phi_i v_i P_i(q) \quad (i = 1,\ 2) \tag{8}$$

$$P_i(q) = \frac{2}{u_i^2}[\exp(-u_i) + u_i - 1] \tag{9}$$

where $u_i = q^2(R_{g,i})^2$ and $R_{g,i} = N_i l_i/6^{1/2}$. $R_{g,i}$ is the radius of gyration for a chain of species i. N_1 is taken to be unity, and $P_1(q) = 1$ at all values of q due to the lack of connectivity between the $scCO_2$ molecules, and

$$V_{ii}(q) = \frac{1}{N_3\phi_3 v_3 P_3(q)} - \frac{2\chi_{i3}}{v_0} \quad (i = 1,\ 2) \tag{10}$$

$$V_{ij}(q) = \frac{1}{N_3\phi_3 v_3 P_3(q)} - \frac{\chi_{i3}}{v_0} - \frac{\chi_{j3}}{v_0} + \frac{\chi_{ij}}{v_0} \quad (i \neq j) \tag{11}$$

The Flory–Huggins interaction parameter, χ_{ij}, quantifies the interactions between species i and j. From our previous work[1] on this system, the functional form of T-dependence of the polymer–polymer interaction parameter is

$$\chi_{23} = 0.092 - 39.60/T \tag{12}$$

Using the absolute M_w values reported in this paper from triple detection to fit the binary polymer–polymer blend data from ref 1, we find that the expression obtained for $\chi_{23}(T)$ changes slightly. This refined expression has been used for all multicomponent mixture analysis described subsequently.

SANS profiles as a function of T and P_{CO_2} from multicomponent mixtures were used to obtain χ_{ij} and l_i by performing nonlinear least-squares fits of the RPA expression (eqs 3–11). Rather than fitting the data by varying l_2 and l_3 independently, a multiplicative constant α is used to adjust both simultaneously:[9,10]

$$l_i(T, P) = \alpha_i(T, P) l_{i,\text{ref}} \quad (i = 2,\ 3) \tag{13}$$

Thus, α can be considered an average expansion factor for SAN and dPMMA which quantifies the effect of T and P_{CO_2} on chain configuration.

4. RESULTS AND DISCUSSION

The solubility of $scCO_2$ in SAN copolymer with $w_{AN} = 0.26$ is shown in Figure 1a where the weight fraction of $scCO_2$ in the copolymer, w_{1-2}, is plotted as a function of P_{CO_2} at the experimental values of T (including 40 °C, as discussed in ref 1). A similar plot of the solubility of $scCO_2$ in hydrogenous PMMA (hPMMA) is shown in Figure 1b, where w_{1-3} is plotted as a function of P_{CO_2} at the experimental values of T. It is evident that w_{1-3} is significantly greater than w_{1-2} at low T. As T increases, the difference in solubility decreases and, at 100 °C, w_{1-2} surpasses w_{1-3} for $P_{CO_2} > 30$ MPa. The swelling of SAN copolymer and dPMMA by $scCO_2$, S_{1-i}, in terms of the percentage change in volume relative to the initial, $scCO_2$-free, volume, is provided as Figure S2. This quantity can be obtained from the ratio of $scCO_2$ and polymer volume fractions in the binary mixture, ϕ_1/ϕ_i, assuming $\Delta V_{mix} = 0$.

The measurements were made on commercial polymers with similar M_w to that use for scattering experiments. It was noted that the solubility of $scCO_2$ in SAN and hPMMA is independent of M_w in the range of molecular weights of interest. We use the data in Figure 1 to interpret SANS data from $scCO_2$/SAN/dPMMA mixtures, neglecting the possible effect of deuteration on the solubility.

The characteristics of the polymers used in this study, SAN87(26) and dPMMA190, are summarized in Table 1, where we report the M_w, PDI, w_{AN}, and N for the SAN copolymer and M_w, PDI, and N for dPMMA. The experiments described herein focus on a single composition of the $scCO_2$-free blend, where the multicomponent mixture composition depends on T and P_{CO_2} determined from the solubility data in Figure 1.

dx.doi.org/10.1021/ma5018154 | Macromolecules 2014, 47, 8089–8097

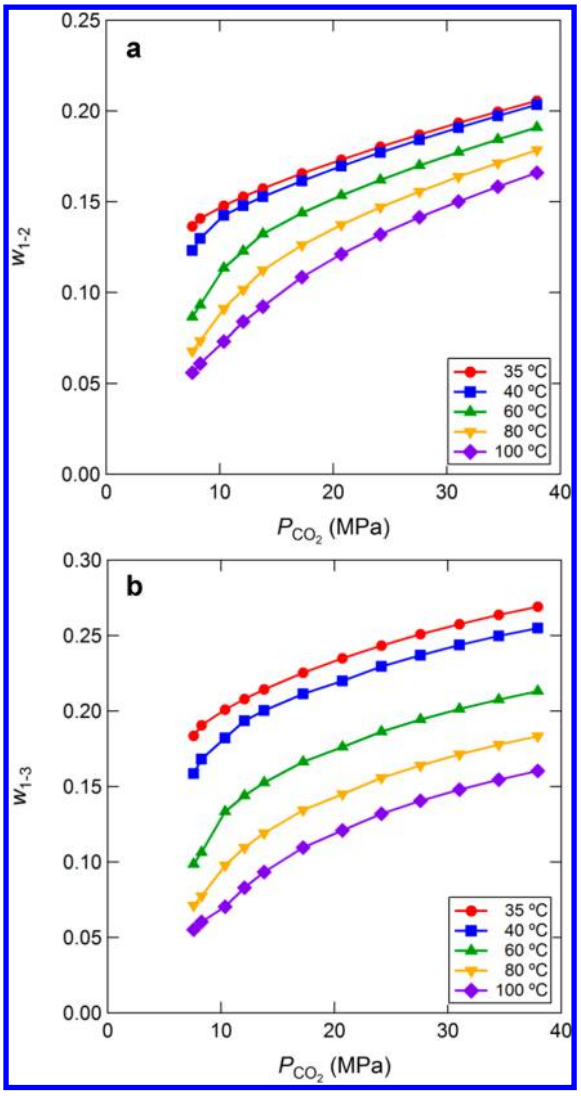

Figure 1. Supercritical carbon dioxide solubility in SAN copolymer (w_{AN} = 0.26) (a) and hydrogenous poly(methyl methacrylate) (b) as a function of P_{CO_2} at the experimental values of T. Solubility is expressed as weight fraction w_{1-i}, where 1 = $scCO_2$, 2 = SAN, and 3 = hPMMA.

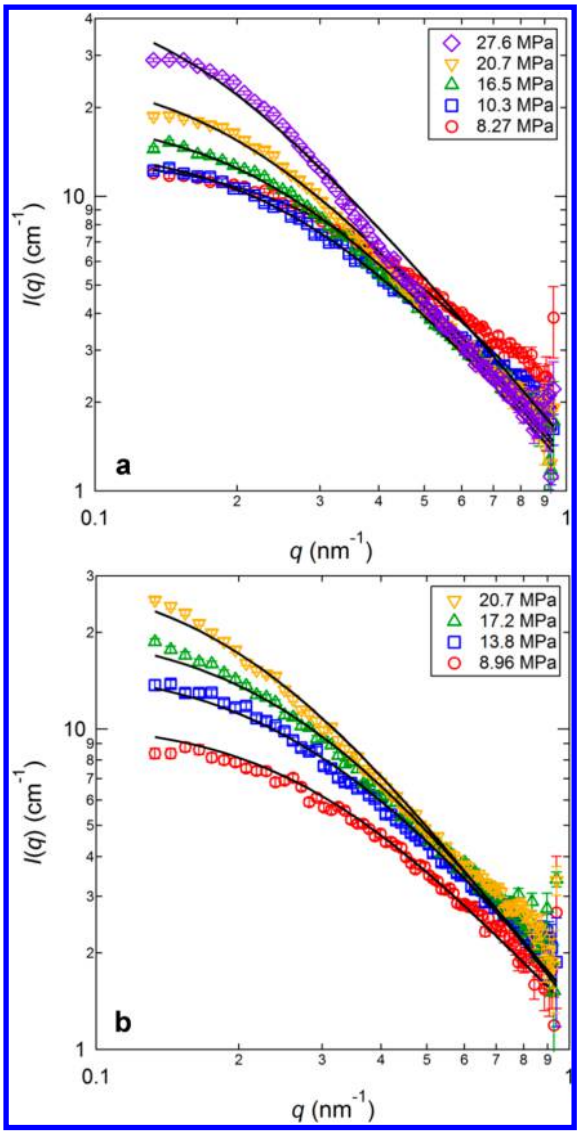

Figure 2. SANS profiles obtained for the multicomponent mixture for isothermal pressure scans at T = 35 °C (a) and T = 100 °C (b). The solid lines are multicomponent RPA fits to the data with χ_{13} and α as adjustable parameters.

Isothermal P_{CO_2} scans were performed on different samples of the same blend at T = 35, 60, 80, and 100 °C. Representative plots of $I(q)$ vs q are shown in Figure 2 for T = 35 and 100 °C for a range of P_{CO_2} which yield homogeneous mixtures. The solid curves in Figure 2 represent the RPA fits to the data. It is evident that the data are in agreement with the predictions of RPA. The profiles (both theoretical and experimental) contain signatures of phase separation, induced by increasing P_{CO_2}. SANS profiles obtained at pressures above 31.0 MPa at 35 °C were clearly time-dependent, indicating the onset of phase separation, and attempts to fit the data with RPA resulted in an unphysical pole in the theoretical profile. The experimentally obtained phase separation pressure, $P_{CO_2,s,expt}$, is thus taken to be 33 ± 2 MPa at 35 °C. Similarly, SANS profiles obtained at pressures above 20.7 MPa at 100 °C were time-dependent. The RPA is only applicable to single phase systems. Scattering profiles at 60 and 80 °C are qualitatively similar and shown in the Supporting Information (Figure S1). The magnitude of the scattering contrast between dPMMA and the two other components (B_{13} and B_{23}) is much larger than that between SAN and $scCO_2$ (B_{12}); the dependence of the scattering length densities on P_{CO_2} and T is given in ref 1. This suggests that the observed phase separation reflects demixing of dPMMA and SAN. The distribution of $scCO_2$ between the polymers is not obvious, especially due to the kinetic limitations of macrophase separation of the polymers. Contrast matching experiments could be used to provide insight into the nature of $scCO_2$ partitioning between the nascent phases.

We can also determine the location of a phase boundary through a Zimm-type analysis if the phase transition is second order. In Figure 3a, $1/I(q)$ vs q^2 for data in the low-q regime are plotted as a function of P_{CO2} at 35 °C. Linear fits to this data allow extrapolation to q = 0 nm^{-1} to obtain estimates of $I(q=0)$ = I_0. These values I_0, when plotted as a function of P_{CO_2} as in Figure 3b, provide a method to determine the phase separation pressure $P_{CO_2,s}$ of the multicomponent mixture. In the case of T = 35 °C, we find that $1/I_0$ = 0 at $P_{CO_2,s,Zimm}$ = 35.6 ± 0.8 MPa.

dx.doi.org/10.1021/ma5018154 | Macromolecules 2014, 47, 8089−8097

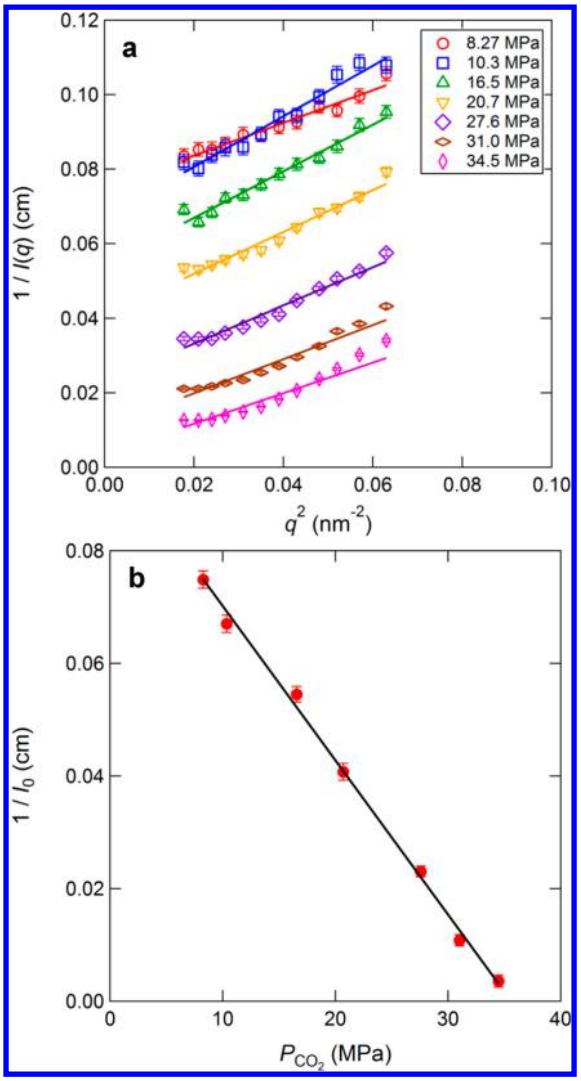

Figure 3. (a) Zimm format plot ($1/I$ vs q^2) of SANS data in the low-q regime for the multicomponent mixture at 35 °C. Solid lines are least-squares linear fits to the data sets. (b) Extrapolated reciprocal scattering intensity $1/I(q = 0) = 1/I_0$ plotted against P_{CO_2} at T = 35 °C. The solid line is a least-squares linear fit used to estimate $P_{CO_2,s,Zimm}$, equal to 35.6 ± 0.8 MPa.

$P_{CO_2,s,Zimm}$ may be interpreted as the spinodal pressure. This agrees well with our observed phase separation at $P_{CO_2,s,expt}$ = 33 ± 2 MPa.

The SANS data obtained at all T were analyzed using the method described in the preceding paragraph. The phase behavior of the particular scCO$_2$/SAN/dPMMA blend of interest in a plot of T vs P_{CO_2} is shown in Figure 4. The values of $P_{CO_2,s,expt}$ and $P_{CO_2,s,Zimm}$ separate the single-phase and phase-separated regions of the phase diagram. The quantitative agreement between $P_{CO_2,s,expt}$ and $P_{CO_2,s,Zimm}$ at all values of T indicates the absence of a metastable window, typically found between two stable thermodynamic states in multicomponent (and binary) mixtures. Since such a window is required by the Gibbs phase rule for first-order phase transitions, we conclude that either this window is narrower than the steps used in this study or that the homogeneous-to-phase-separation transition is a second-order phase transition over the entire temperature

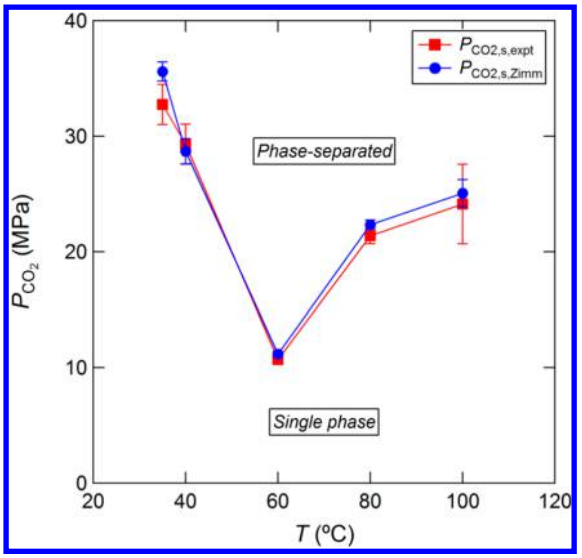

Figure 4. Phase separation pressure $P_{CO_2,s}$ as a function of T for the scCO$_2$/SAN/dPMMA blend. Red squares represent $P_{CO_2,s,expt}$ estimated from experimental observation, and blue circles represent $P_{CO_2,s,Zimm}$ calculated from Zimm analysis of scattering data. Lines are provided to guide the eye.

and pressure window. The values of $P_{CO_2,s,expt}$ and $P_{CO_2,s,Zimm}$ for each T are listed in Table 4. The phases separation pressure,

Table 4. Phase Separation Conditions for ScCO$_2$/SAN/dPMMA Blends

T (°C)	$P_{CO_2,s,expt}$ (MPa)	$P_{CO_2,s,Zimm}$ (MPa)
35	33 ± 2	35.6 ± 0.8
40	30 ± 2	29 ± 1
60	11.4 ± 0.3	11.2 ± 0.2
80	21.4 ± 0.7	22.3 ± 0.2
100	24 ± 3	25 ± 1

$P_{CO_2,s}$ (which we take as $P_{CO_2,s,Zimm}$ from this point forward), is a nonmonotonic function of T: it decreases with increasing T in the low-T limit (below 60 °C) but increases with increasing T in the high-T limit (above 60 °C).

This nonmonotonic phase boundary in Figure 4 is unusual but can be qualitatively explained on the basis of the interactions between the three constituent species. At low T, SAN and dPMMA are highly miscible (χ_{23} = −0.366), and thus high P_{CO_2} is required to induce phase separation. As T increases, the miscibility between SAN and dPMMA decreases (χ_{23} = −0.142 at 100 °C), and less scCO$_2$ is required to induce phase separation. However, as T increases further, the solubility of scCO$_2$ in the polymers also decreases (see Figure 1). Since the phase separation is induced by the uptake of scCO$_2$, a higher value of P_{CO_2} is needed to induce the phase transition at higher T.

It is unlikely that hydrostatic pressure is an important variable in this study. We were unable to find explicit studies of the effect of hydrostatic pressure on the thermodynamics of SAN/PMMA mixtures. In the well-studied case of mixtures of polymethylbutylene and polyethylbutylene, the phase separation temperature T_s was observed to shift by 40 °C under the influence of applied P greater than 300 MPa.[9,10] In our case T_s

dx.doi.org/10.1021/ma5018154 | Macromolecules 2014, 47, 8089−8097

changes by as much as 125 °C when equilibrated with a $scCO_2$ reservoir with P_{CO_2} = 33 MPa (T_s for this blend in the $scCO_2$-free state is ~160 °C).[1] It is thus appropriate to consider the effect of ρ_{CO_2}, the density of the $scCO_2$ in the reservoir instead of P_{CO_2}.[11] Figure 5 shows the $scCO_2$/SAN/dPMMA blend

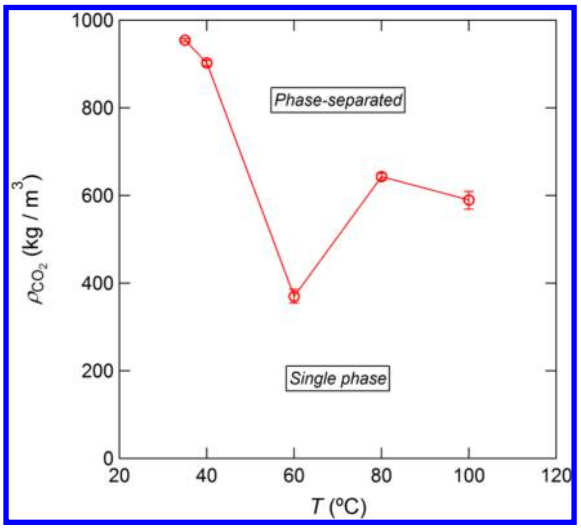

Figure 5. Phase separation density $\rho_{CO_2,s}$ as a function of T for the multicomponent mixture, with $\rho_{CO_2,s}$ determined from $P_{CO_2,s}$ at each experimental T. The solid line is provided to guide the eye.

phase behavior on a ρ_{CO_2} vs T plot. The phase diagrams shown in Figures 4 and 5 are qualitatively similar to nonmonotonic dependences of the phase separation pressure and density on temperature.

We now return to the multicomponent RPA fits shown in Figures 1 and 2, which enable determination of the Flory–Huggins interaction parameters between $scCO_2$ and each polymer (χ_{12} and χ_{13}) as described in ref 1. Both $scCO_2$ uptake and SANS data are needed to obtain the two parameters unambiguously as the SANS data alone are consistent with two pairs of χ_{12} and χ_{13} values. Figure 6 shows the dependence of χ_{13} on P_{CO_2} at the values of T investigated. The data fall into two regimes: a low-T regime $T \leq 40$ °C in the vicinity of the CO_2 critical temperature and a second farther away from critical temperature, $T \geq 60$ °C. In the low-T regime, χ_{13} increases monotonically with P_{CO_2}, asymptotically approaching a plateau value of about 2.4. Conversely, in the high-T regime, χ_{13} goes through a minimum ($\chi_{13} \approx 0.3$ near P_{CO_2} = 9 MPa for 60 °C $\leq T \leq$ 100 °C) before increasing toward the plateau value. Data ranges in Figure 6 are limited by the location of the phase boundary, since χ_{13} can only be determined for homogeneous mixtures where the RPA applies.

In Figure 7, the difference between $scCO_2$–polymer interaction parameters, $\chi_{13} - \chi_{12}$, are plotted as a function of $P_{CO_2,s}$ for all T. For nearly all T and P_{CO_2} considered, $\chi_{13} - \chi_{12}$ is small and negative, indicating that dPMMA has more favorable interactions with $scCO_2$ than SAN. The exception to this condition is found for $P_{CO_2,s}$ < 8.96 MPa where near $\chi_{13} - \chi_{12}$ is relatively large and positive. We do not have an explanation for this observation.

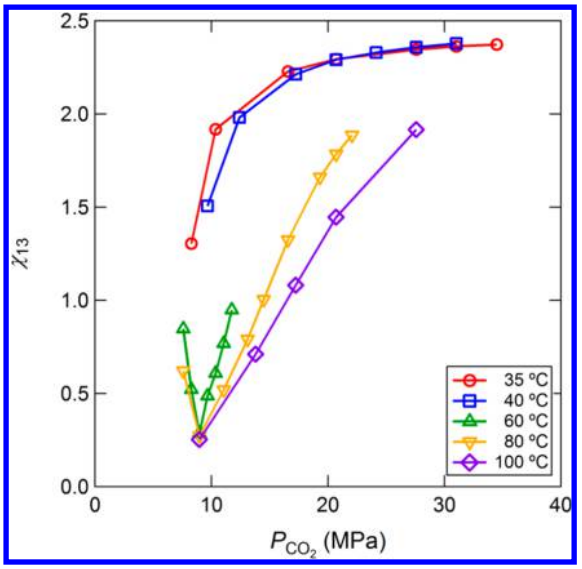

Figure 6. Pairwise interaction parameter for $scCO_2$ and dPMMA190, χ_{13}, obtained from scattering profiles of the multicomponent mixture, as a function of P_{CO_2}, at all experimental T: 35 °C (red circles), 40 °C (blue squares), 60 °C (green up-triangles), 80 °C (yellow down-triangles), 100 °C (purple diamonds). 1 = $scCO_2$ and 3 = dPMMA. Solid lines are provided to guide the eye. The error bars for each value of χ_{13}, representing one standard deviation in the measured value, are within the size of the data symbols in this figure.

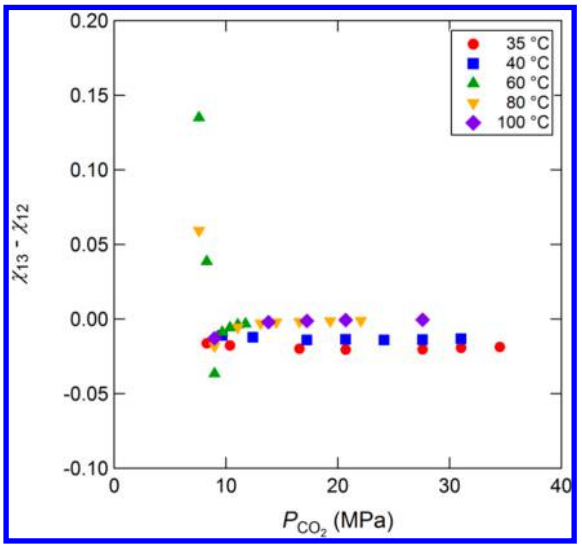

Figure 7. Difference in $scCO_2$–polymer interaction parameters, $\chi_{13} - \chi_{12}$, plotted as a function of P_{CO_2}, at all experimental T: 35 °C (red circles), 40 °C (blue squares), 60 °C (green up-triangles), 80 °C (yellow down-triangles), and 100 °C (purple diamonds). 1 = $scCO_2$, 2 = SAN, and 3 = dPMMA.

Figure 8 shows plots of χ_{12} and χ_{13} against ρ_{CO_2}. The data appear to collapse onto a straight line. Least-squares fits to the data yield

$$\chi_{12} = 0.0028\rho_{CO_2} - 0.099 \quad (14)$$

$$\chi_{13} = 0.0027\rho_{CO_2} - 0.075 \quad (15)$$

While there is a strong correlation between ρ_{CO_2} and both χ_{12} and χ_{13}, it is unlikely that density alone determines the

dx.doi.org/10.1021/ma5018154 | Macromolecules 2014, 47, 8089–8097

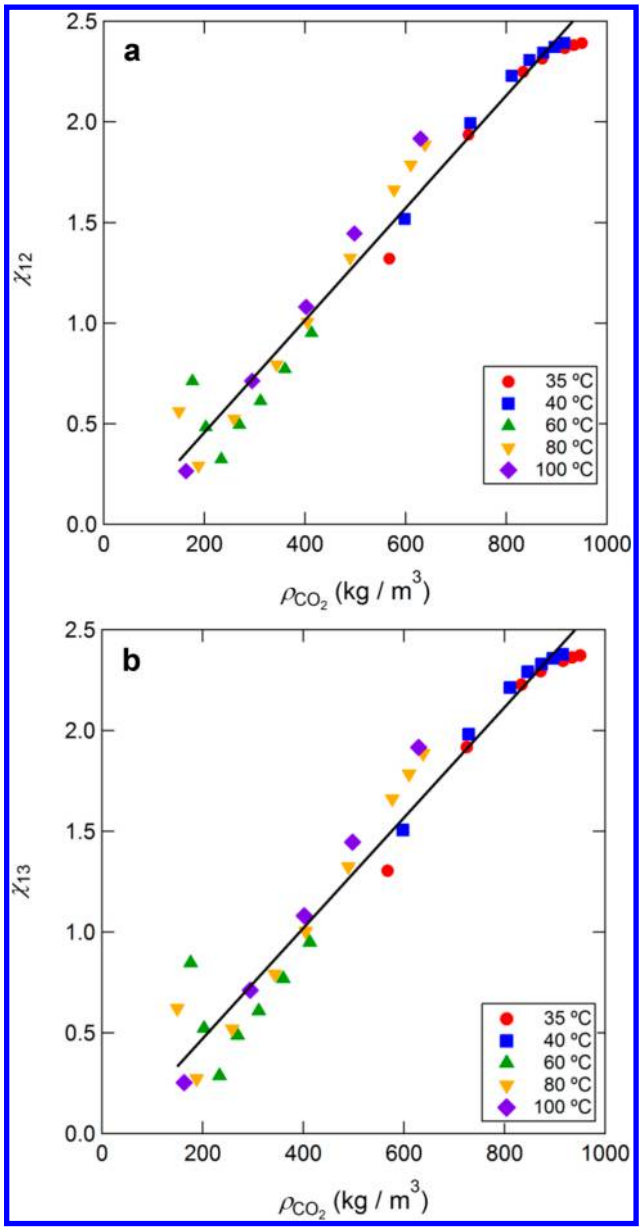

Figure 8. (a) $scCO_2$–dPMMA190 interaction parameter χ_{12} and (b) $scCO_2$–SAN87(26) interaction parameter χ_{13} plotted as a function of ρ_{CO_2}, at all T: 35 °C (red circles), 40 °C (blue squares), 60 °C (green up-triangles), 80 °C (yellow down-triangles), 100 °C (purple diamonds). The solid lines are least-squares linear fits to the full data sets, yielding the relationships $\chi_{13} = 0.0027\rho_{CO_2} - 0.075$ and $\chi_{12} = 0.0028\rho_{CO_2} - 0.099$.

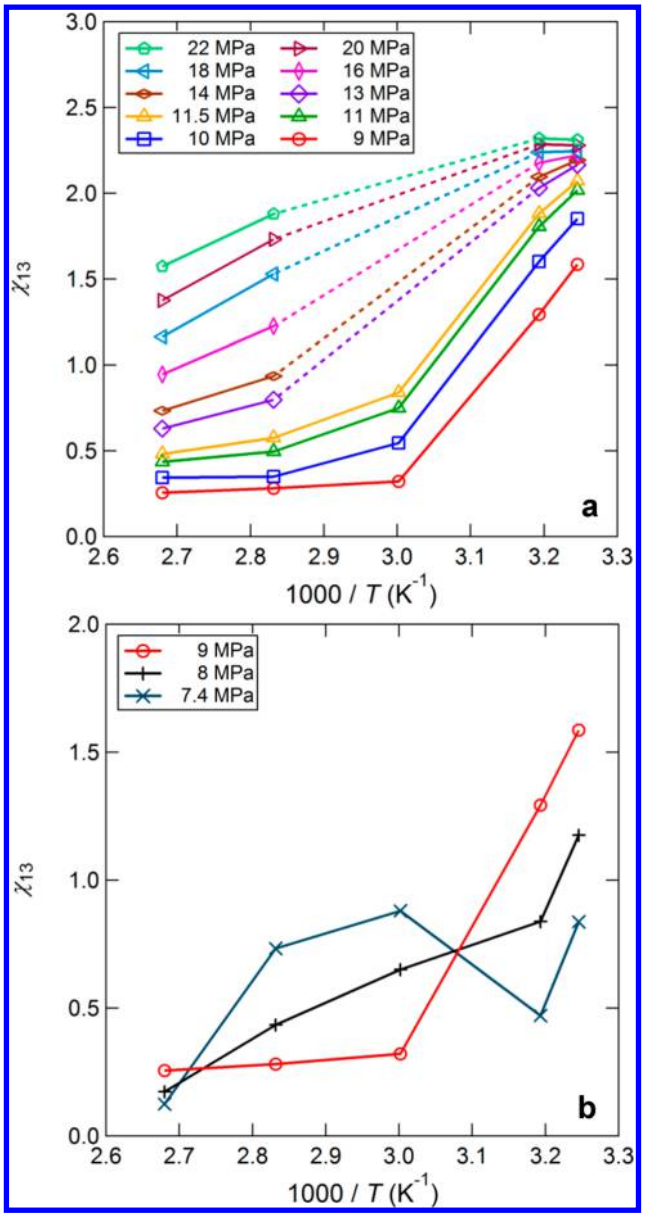

Figure 9. (a) $scCO_2$–PMMA185 interaction parameter χ_{13} plotted vs $1000/T$, over the range 9 MPa $\leq P_{CO_2} \leq$ 22 MPa. Solid lines are provided to guide the eye. Dashed lines cover the region where the mixture at 60 °C has undergone macrophase separation (>11.5 MPa). (b) $scCO_2$–PMMA185 interaction parameter χ_{13} plotted vs $1000/T$, over the range 7.4 MPa $\leq P_{CO_2} \leq$ 9 MPa. Solid lines are provided to guide the eye.

thermodynamic interactions between $scCO_2$ and the polymers of interest. Note that miscibility is greater (i.e., χ_{13} is lower) when $scCO_2$ has gas-like densities. It is likely that the measured interactions account for interplay between molecular interactions as well as the unique features of CO_2 in the supercritical regime, including density fluctuations. It is important to note that our analysis applies to ternary $scCO_2$/SAN/dPMMA mixtures. Whether or not these interaction parameters apply to binary $scCO_2$/SAN and $scCO_2$/dPMMA is unclear.

In the literature, χ parameters are often plotted as a function of inverse T. In Figure 9a, we plot χ_{13} against $1000/T$ over the range 9 MPa $\leq P_{CO_2} \leq$ 22 MPa. At P_{CO_2} = 9 MPa, there appear to be two regimes: χ_{13} is roughly independent of T for $T \geq 60$ °C but increases linearly with $1000/T$ for $T > 60$ °C. The latter dependence is typically observed in polymer/polymer and polymer/solvent systems. As P_{CO_2} increases, the distinction between the two regimes becomes less pronounced. At high P_{CO_2}, χ_{13} appears to be approximately a linear function of $1000/T$. (Missing data in Figure 9 are due to phase separation.) χ_{13} vs $1000/T$ plots at P_{CO_2} below 9 MPa are much more complex and thus shown separately in Figure 9b. At P_{CO_2} very close to the critical pressure of CO_2, there appear to be three separate regimes, with χ_{13} increasing with $1/T$ at high temperatures (low

dx.doi.org/10.1021/ma5018154 | Macromolecules 2014, 47, 8089–8097

$1/T$), decreasing with $1/T$ at intermediate temperatures, and increasing again with $1/T$ at low temperatures.

The reason for the behaviors seen in Figures 7−9 is not obvious. While complex phase behavior in the presence of $scCO_2$ is reported widely in the literature,[12−20] there have been relatively few attempts to explain observations in terms of underlying intermolecular interactions.[21−25] In an important study, Koga et al. used neutron reflectivity to investigate the swelling of thin polymer films by $scCO_2$ and found a remarkably similar nonmonotonic trend of $\chi_{CO_2\text{-polymer}}$ on P_{CO_2} to that reported here in Figure 6, albeit at only a single T.[26,27] Those authors attributed the unusual behavior to the dramatic density fluctuations which occur near the critical regime of $scCO_2$ as a result of the "density fluctuation ridge". As ρ_{CO_2} increases at a given T, the density fluctuations of neat $scCO_2$, given by $\langle(\Delta n)^2\rangle/\langle n\rangle$ where n is the number of molecules, go through a maximum. The locus of these maxima forms a "ridge" in a P_{CO_2} vs T plot. While the magnitude of $\langle(\Delta n)^2\rangle/\langle n\rangle$ decreases along the ridge as T increases, the generality of the feature could influence the observed behavior even at conditions well removed from the regime of critical density fluctuations.

There are many theories that address phase behavior of $scCO_2$/polymer mixtures.[28−36] To our knowledge, all of them are restricted to binary mixtures containing a single polymeric species. In future work, we will attempt to see if any of these theories provide insight into the χ parameters presented in this study.

5. CONCLUSIONS

We present results from SANS experiments of a multicomponent mixture composed of $scCO_2$, SAN, and dPMMA, equilibrated in contact with a reservoir of $scCO_2$ at fixed T and P_{CO_2}. At constant T, the mixtures phase separated as P_{CO_2} of the reservoir was increased. $P_{CO_2,s}$ was found to be a nonmonotonic function of T with a sharp minimum at T = 60 °C. The intermolecular interactions responsible for this nontrivial phase behavior were determined from neutron scattering experiments on the ternary mixtures and $scCO_2$ uptake measurements in each neat polymer. A formalism of the multicomponent random phase approximation was used to obtain the dependence of the $scCO_2$−polymer interaction parameters on T, P_{CO_2}, and ρ_{CO_2} from the SANS measurements. At low T, interaction parameters increased monotonically to a plateau level with respect to P_{CO_2}, while interaction parameters measured at higher T go through a minimum. The interaction parameters collapsed onto a straight line when plotted as a function of ρ_{CO_2}.

■ ASSOCIATED CONTENT

Supporting Information

Figures S1 and S2. This material is available free of charge via the Internet at http://pubs.acs.org.

■ AUTHOR INFORMATION

Corresponding Author

*E-mail nbalsara@berkeley.edu, phone (510) 642-8937 (N.P.B.).

Notes

The authors declare no competing financial interest.

■ ACKNOWLEDGMENTS

We acknowledge The Dow Chemical Company for providing the primary support for this work and thank Dr. Alan Nakatani and Dr. Tirtha Chatterjee for educational discussions on the design and interpretation of SANS experiments. Prof. Ram Gupta and Prof. Isaac Sanchez are acknowledged for helpful discussions on the interpretation of the results. Dr. Boualem Hammouda, Mr. Cedric Gagnon, and Mr. Juscelino Leao of the NIST Center for Neutron Research are thanked for their assistance in carrying out SANS experiments. We acknowledge the support of the National Institute of Standards and Technology, U.S. Department of Commerce, in providing the neutron research facilities used in this work. This work utilized facilities supported in part by the National Science Foundation under Agreement DMR-0454672.

■ NOMENCLATURE

Abbreviations

AN	acrylonitrile
dPMMA	deuterated poly(methyl methacrylate) homopolymer
PMMA	poly(methyl methacrylate) homopolymer
RPA	random phase approximation
S	styrene
SAN	styrene−acrylonitrile random copolymer
SANS	small-angle neutron scattering
$scCO_2$	supercritical carbon dioxide
THF	tetrahydrofuran

Symbols

B	neutron scattering length contrast, nm^{-2}
b	neutron scattering length, nm
d	MSB polymer sample diameter, mm
$I(q)$	coherent scattered neutron intensity, cm^{-1}
I_0	scattering intensity extrapolated to $I(q = 0\ nm^{-1})$, cm^{-1}
K	Boltzmann constant, 1.38×10^{-23} J/K
$k_{a,ij}$	PC-SAFT interaction parameter coefficient, −
$k_{b,ij}$	PC-SAFT interaction parameter coefficient, K^{-1}
l	statistical segment length, nm
$l_{i,ref}$	statistical segment length at T_{ref} and P_{ref}, nm
M_0	monomer molecular weight, kg/mol
M_n	number-averaged molecular weight, kg/mol
M_w	weight-averaged molecular weight, kg/mol
m	PC-SAFT segments per chain, −
m_p	MSB polymer sample mass, kg
N	number of effective monomer units of size 0.1 nm^3 in a given chain, −
n	number of molecules, −
P	pressure, MPa
P_{CO_2}	CO_2 bath pressure, MPa
$P_i(q)$	single-chain form factor for species i, −
P_{ref}	reference pressure, 0.1 MPa
PDI	polydispersity index, −
q	scattering vector, nm^{-1}
R_g	radius of gyration of species i, nm
$S_{ij}(q)$	complete structure factor for species i and j, nm^3
$S^{\circ}_{ij}(q)$	partial structure factor for species i and j, nm^3
T	absolute temperature, K
T_{ref}	reference temperature, 413.15 K
t	film thickness, μm
V_b	MSB experiment container volume, m^3
$V_{ij}(q)$	interaction structure factor for species i and j, nm^{-3}
V_{mix}	MSB experiment swollen polymer volume, m^3

v monomer volume for species i, nm^3
v_0 monomer unit reference volume, 0.1 nm^3
w_{AN} copolymer composition in weight fraction acrylonitrile monomer, −
$x_g^{PC\text{-}SAFT}$ PC-SAFT CO_2 fraction in swollen polymer, −

Greeks

α chain expansion factor, −
ε PC-SAFT dispersion energy, J
θ scattering angle, rad
λ neutron wavelength, nm
ρ density, kg/m^3
ρ_f MSB experiment fluid density, kg/m^3
$\rho_{mix}^{PC\text{-}SAFT}$ PC-SAFT swollen polymer density, kg/m^3
σ PC-SAFT segment diameter, nm
ϕ blend volume fraction, −
χ_{ij} Flory−Huggins interaction parameter for species i and j, −

Subscripts

i blend constituent species (1 = $scCO_2$, 2 = SAN, 3 = PMMA)
$1-i$ $scCO_2$ in a binary mixture with i = 2 (SAN) or 3 (PMMA)
s condition for phase separation

REFERENCES

(1) Inceoglu, S.; Young, N. P.; Jackson, A. J.; Kline, S. R.; Costeux, S.; Balsara, N. P. *Macromolecules* **2013**, *46*, 6345−6356.
(2) Certain commercial equipment, instruments, materials, and suppliers are identified in this paper to foster understanding. Such identification does not imply recommendation or endorsement by the National Institute of Standards and Technology, nor does it imply that the materials or equipment identified are necessarily the best available for the purpose.
(3) Eitouni, H. B.; Balsara, N. P. In *Physical Properties of Polymers Handbook*, 2nd ed.; Mark, J. E., Ed.; AIP Press: Woodbury, NY, 2007; p 339.
(4) Wen, G.; An, L. *J. Appl. Polym. Sci.* **2003**, *90*, 959−962.
(5) Areerat, S.; Funami, E.; Hayata, Y.; Nakagawa, D.; Ohshima, M. *Polym. Eng. Sci.* **2004**, *44*, 1915−1924.
(6) Gross, J.; Sadowski, G. *Ind. Eng. Chem. Prod. Res.* **2001**, *40*, 1244−1260.
(7) Kline, S. R. *J. Appl. Crystallogr.* **2006**, *39*, 895−900.
(8) Balsara, N. P.; Lohse, D. J.; Graessley, W. W.; Krishnamoorti, R. *J. Chem. Phys.* **1994**, *100*, 3905−3910.
(9) Lefebvre, A. A.; Lee, J. H.; Balsara, N. P.; Hammouda, B. *Macromolecules* **2000**, *33*, 7977−7989.
(10) Lefebvre, A. A.; Balsara, N. P.; Lee, J. H.; Vaidyanathan, C. *Macromolecules* **2002**, *35*, 7758−7764.
(11) Span, R.; Wagner, W. *J. Phys. Chem. Ref. Data* **1996**, *25*, 1509−1596.
(12) Walker, T.; Raghavan, S. R.; Royer, J. R.; Smith, S. D.; Wignall, G. D.; Melnichenko, Y.; Khan, S. A.; Spontak, R. J. *J. Phys. Chem. B* **1999**, *103*, 5472−5476.
(13) Watkins, J. J.; Brown, G. D.; RamachandraRao, V. S.; Pollard, M. A.; Russell, T. P. *Macromolecules* **1999**, *32*, 7737−7740.
(14) Vogt, B. D.; Brown, G. D.; RamachandraRao, V. S.; Watkins, J. J. *Macromolecules* **1999**, *32*, 7907−7912.
(15) RamachandraRao, V. S.; Watkins, J. J. *Macromolecules* **2000**, *33*, 5143−5152.
(16) Vogt, B. D.; RamachandraRao, V. S.; Gupta, R. R.; Lavery, K. A.; Francis, T. J.; Russell, T. P.; Watkins, J. J. *Macromolecules* **2003**, *32*, 4029−4036.
(17) Francis, T. J.; Vogt, B. D.; Wang, M. X.; Watkins, J. J. *Macromolecules* **2007**, *40*, 2515−2519.
(18) Chandler, C. M.; Vogt, B. D.; Francis, T. J.; Watkins, J. J. *Macromolecules* **2009**, *42*, 4867−4873.
(19) Shinkai, T.; Ito, M.; Sugiyama, K.; Ito, K.; Yokoyama, H. *Soft Matter* **2012**, *8*, 5811−5817.
(20) Shinkai, T.; Ito, M.; Sugiyama, K.; Ito, K.; Yokoyama, H. *Soft Matter* **2013**, *9*, 10689−10693.
(21) RamachandraRao, V. S.; Vogt, B. D.; Gupta, R. R.; Watkins, J. J. *J. Polym. Sci., Part B: Polym. Phys.* **2003**, *33*, 5143−5152.
(22) Walker, T.; Melnichenko, Y.; Wignall, G. D.; Spontak, R. J. *Macromolecules* **2003**, *36*, 4245−4249.
(23) Walker, T.; Colina, C. M.; Gubbins, K. E.; Spontak, R. J. *Macromolecules* **2004**, *37*, 2588−2595.
(24) Li, Y.; Wang, X.; Sanchez, I. C.; Johnston, K. P.; Green, P. F. *J. Phys. Chem. B* **2007**, *111*, 16−25.
(25) Shi, L.-Y.; Shen, Z.; Fan, X.-H. *Macromolecules* **2011**, *44*, 2900−2907.
(26) Koga, T.; Seo, Y.-S.; Zhang, Y.; Shin, K.; Kusano, K.; Nishikawa, K.; Rafailovich, M. H.; Sokolov, J. C.; Chu, B.; Pfeiffer, D.; Occhiogrosso, R.; Satija, S. K. *Phys. Rev. Lett.* **2002**, *89*, 125506-1−4.
(27) Koga, T.; Seo, Y.-S.; Shin, K.; Zhang, Y.; Rafailovich, M. H.; Sokolov, J. C.; Chu, B.; Satija, S. K. *Macromolecules* **2003**, *36*, 5236−5243.
(28) Kiszka, M. B.; Meilchen, M. A.; McHugh, M. A. *J. Appl. Polym. Sci.* **1988**, *36*, 583−597.
(29) Garg, A.; Gulari, E.; Manke, C. W. *Macromolecules* **1994**, *27*, 5643−5653.
(30) Gromov, D. G.; de Pablo, J. J.; Luna-Barcenas, G.; Sanchez, I. C.; Johnston, K. P. *J. Chem. Phys.* **1998**, *108*, 4647−4653.
(31) Tumakaka, F.; Gross, J.; Sadowski, G. *Fluid Phase Equilib.* **2002**, *194−197*, 541−551.
(32) Shin, H. Y.; Wu, J. Z. *Ind. Eng. Chem. Res.* **2010**, *49*, 7678−7684.
(33) Xu, X.; Cristancho, D. E.; Costeux, S.; Wang, Z.-G. *Ind. Eng. Chem. Res.* **2012**, *51*, 3832−3840.
(34) Xu, X.; Cristancho, D. E.; Costeux, S.; Wang, Z.-G. *J. Chem. Phys.* **2012**, *137*, 054902-1−8.
(35) Hossain, M. Z.; Yuan, Y.; Teja, A. S. *Ind. Eng. Chem. Res.* **2013**, *52*, 12654−12660.
(36) DeFelice, J.; Lipson, J. E. G. *Macromolecules* **2014**, *47*, 5643−5654.